Highlights of DØ QCD related analyses

Lars Sonnenschein

RWTH Aachen University, III. Phys. Inst. A, 52056 Aachen, Germany

E-mail: `Lars.Sonnenschein@cern.ch`

Abstract. DØ provides a wealth of measurements conceived for probing perturbative and non-perturbative aspects of QCD, giving an accurate experimental account for Standard Model production processes including jets, leptons and photons and improving the sensitivity and the understanding in search for new physics. Among the most important subjects are inclusive jet production, vector boson plus jet production, direct photon production and measurements in Minimum Bias events and Double Parton Scattering which are discussed here and compared to theory predictions.

1. Introduction

Proton anti-proton collisions at a centre of mass energy of $\sqrt{s} = 1.96$ TeV are taking place at the the Tevatron accelerator, Fermilab. A peak luminosity of $4.3 \cdot 10^{32}$ cm^{-}2s^{-1} has been reached and over 11.6 fb^{-1} integrated luminosity are already delivered, of which 10.5 fb^{-1} have been recorded by the DØ experiment. The presented analyses are based on integrated luminosities ranging between 0.7 and 4.2 fb^{-1}.

The DØ detector [1] has broad particle identification capabilities. Jets, electrons and photons are detected by the calorimeter with fine granularity ($\Delta\eta \times \Delta\phi \sim 0.1 \times 0.1$) an add "the" resolution. Charged particles are reconstructed by means of the central tracking system and muons are detected in the muon spectrometer as outermost detector component. The data taking efficiency is $\geq 90\%$ (in Run 2b it is about 92%, on average).

Jet measurements are well understood by Quantum Chromodynamics (QCD) calculations. They can be exploited to set constraints on the non-perturbative Parton Distribution Functions (PDF's). In the kinematic plane of proton momentum fraction x and virtuality scale Q^2, regions accessible to fixed target experiments, HERA, the Tevatron and LHC are complementary. Only Tevatron inclusive jet data provide significant constraints at high x and Q^2. Jet measurements are also important within searches for new phenomena. Heavy particles can decay into quarks which in turn fragment into jets. Extra dimensions and quark compositeness are examples of such new kind of phenomena.

The production of dijets at the Tevatron is dominated by the gluon gluon fusion process at low transverse jet momenta. Toward larger transverse jet momenta the fraction of quark anti-quark annihilation dominates, while the fraction of quark gluon fusion tends to decrease marginally.

Among all past and present hadron colliders the Tevatron inclusive jet production data dominates together with published LHC results the high jet transverse momentum reach. At the same time, the Tevatron has by far the best sensitivity at large (anti-)proton momentum fractions x.

While the data are corrected for detector effects, the predictions take into account non-perturbative contributions due to underlying event and hadronisation. Finally, the comparison to data is then established at the hadronic final state as defined in [4].
The convention speed of light $c \equiv 1$ is adopted throughout this article.

The following section covers inclusive jet production measurements. Section 3 shows two examples of vector boson plus jet production measurements. Section 4 encompasses the most relevant direct photon production measurements of DØ. Important non-perturbative measurements in the regime of Minimum Bias events and Double Parton Scattering are given in section 5.

2. Inclusive jet production

The measurement of the cross section of inclusive jet production in hadron collisions provides stringent tests of QCD. Large jet transverse momenta with respect to the beam axis (p_T) ensure small contributions from long-distance processes and the jet production can be calculated in perturbative QCD (pQCD). The inclusive jet cross section in $p\bar{p}$ collisions provides one of the most direct probes of physics at small distances. In particular, it is directly sensitive to the strong coupling constant (α_s) and the PDF's of the proton. Furthermore it can be exploited to set constraints on the internal structure of quarks [5].

2.1. Inclusive jet production

The double differential inclusive jet production cross section is measured [2] as a function of the leading jet transverse momentum and the rapidity based on an integrated luminosity of 0.7 fb^{-1}. The Run II iterative seed-based cone jet algorithm including mid-points [3] with cone radius $R = \sqrt{(\Delta y)^2 + (\Delta\phi)^2} = 0.7$ in rapidity y and azimuthal angle ϕ space is used to cluster energies deposited in calorimeter towers as well as for the pQCD calculations on the partonic final state. The jet transverse momentum is corrected for the energy response of the calorimeter, energy showering in and out of the jet cone and for additional energy from event pile-up and multiple parton interactions (double parton scattering). Events with jets above a transverse momentum threshold of 50 GeV in the rapidity range of $|y| < 2.4$ are selected. The cross section is measured in six rapidity bins as a function of jet p_T, reaching transverse momenta above 600 GeV. The cross section is corrected for muons and neutrinos, not reconstructed within jets. Corrections for jet migration between bins in p_T and y due to finite resolution in energy and position are determined in an unfolding procedure, based on the experimental p_T and y resolutions. The bin sizes are chosen to minimise migration corrections due to the experimental resolution. The dominant systematic uncertainty comes from the Jet Energy Scale (JES). The steeply falling jet transverse momentum spectrum causes shifts in energy which translate into a large uncertainty on the cross section. The typical JES uncertainty is 1 - 2% which results in a total uncertainty on the cross section of 15 - 30%. Perturbative QCD predictions to next-to-leading order (NLO) in α_s, computed using the FASTNLO program [6], based on NLOJET++ [7] are compared to data making use of PDF's from CTEQ6.5M [8][9][10]. The theoretical uncertainty due to variation of the renormalisation (μ_R) and factorisation (μ_F) scales by a factor of two up and down are of order 10%. The scale itself is chosen to be the individual jet p_T. In all y regions the predictions agree well with the data. The data tends to be lower than the central prediction making use of CTEQ PDF's, in particular at very large transverse jet momentum.

2.2. Inclusive dijet production invariant mass cross section

The inclusive dijet production cross section is measured [11] as a function of the dijet mass based on an integrated luminosity of 0.7 fb^{-1}. This measurement is sensitive to quark compositeness, extra spatial dimensions and undiscovered heavy particles decaying into two quarks. The invariant mass distribution is particularly sensitive to the PDF of gluons at high (anti-)proton

momentum fraction x where the gluon distribution is weakly constrained. The two leading jets (cone algorithm [3] with radius $R = 0.7$) are required to exceed a transverse momentum threshold of 40 GeV. The cross section is measured in different regions of maximal rapidity, defined as $|y|_{\max} = \max(|y_1|, |y_2|)$. The six equidistant disjoint regions are given by: $0 < |y|_{\max} < 0.4$, $0.4 < |y|_{\max} < 0.8$, $0.8 < |y|_{\max} < 1.2$, $1.2 < |y|_{\max} < 1.6$, $1.6 < |y|_{\max} < 2.0$, $2.0 < |y|_{\max} < 2.4$. Calorimeter shower shapes are used to remove remaining background due to electrons, photons and detector noise giving rise to jets. The invariant mass bins are chosen to have a size of about twice the mass resolution and to respect an efficiency and purity of about 50%. The jet p_T resolution is measured in events with exactly two jets and has been found to be approximately 13% (7%) at $p_T \simeq 50$ (400) GeV in the central calorimeter (CC) and the endcap calorimeter (EC) and 16% (11%) at $p_T \simeq 50$ (400) GeV in the inter cryostat region (ICR) between the two calorimeter compartments CC and EC. The total experimental corrections to the data are less than $\pm 2\%$. The systematic uncertainties on the cross section are dominated by the uncertainties in the jet energy calibration which range from 6 - 22% in the endcap to 15 - 45% in the central region. The second largest systematic uncertainty is given by the p_T resolution uncertainty, ranging between 2 and 10% in all regions. The luminosity determination has an uncertainty of 6.1% which is completely correlated across all bins. The data are compared to the NLO prediction computed using [6], based on NLOJET++ [7][13] for MSTW2008NLO PDF's [12] with $\alpha_s(m_Z) = 0.120$. In addition, a comparison to theoretical predictions using CTEQ6.6 PDF's [14] has been made. The difference in cross section due to the choice of PDF's is 40 - 60% at the highest mass. MSTW2008NLO PDF's are favoured. However, its has to be noted that their determination included the DØ inclusive jet production cross section measurement [2] which is based on the same data set as this dijet measurement. A further difference is that the MSTW2008NLO PDF's exclude Tevatron data taken before 2000 in contrast to the CTEQ6.6 PDF's.

2.3. Inclusive 3-jet invariant mass cross section

The inclusive 3-jet production cross section is measured [15] as a function of the invariant 3-jet mass based on an integrated luminosity of 0.7 fb^{-1}. Recent measurements of inclusive jet and dijet production in $p\bar{p}$ collisions at a centre of mass energy of $\sqrt{s} = 1.96$ TeV [16][17][18][2][19][20]

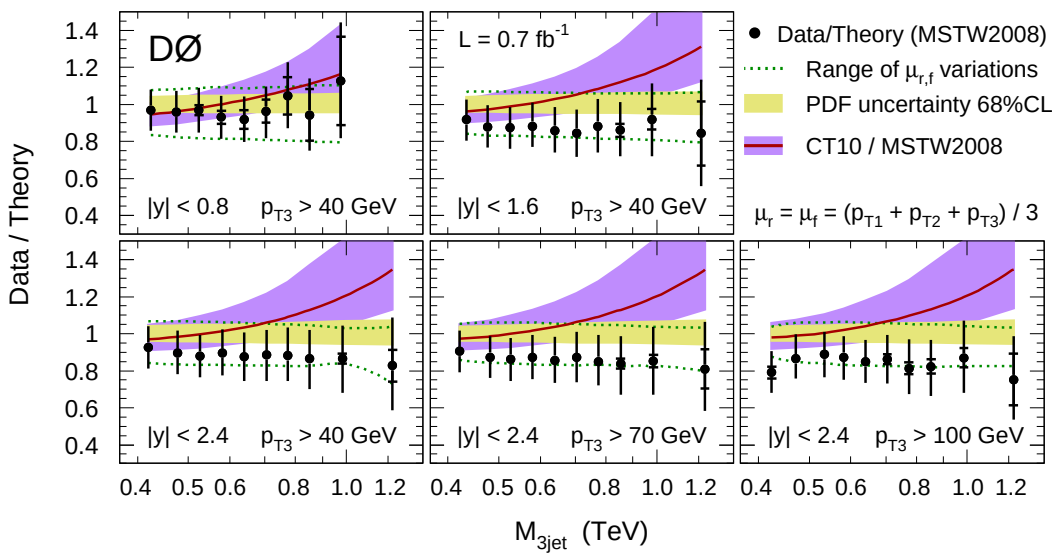

Figure 1. Data over theory ratios of the differential cross section $d\sigma_{3\text{jet}}/dM_{3\text{jet}}$ in the different rapidity regions and for different third leading jet transverse momentum requirements. The pQCD predictions are given for two different PDF's.

have been used to determine α_s [21] and the proton PDF's and to set limits on a number of physics models beyond the standard model [22][23][24]. This shows the successful pQCD description of observables which are directly sensitive to matrix elements of $\mathcal{O}(\alpha_s^2)$. Testing pQCD at higher orders of α_s requires measuring cross sections of higher jet multiplicities. The three jet cross section is directly sensitive to matrix elements of $\mathcal{O}(\alpha_s^3)$ while the PDF sensitivity is similar. Due to the fact the pQCD calculations are available to next-to-leading order (NLO) in α_s [25][26][7][13], the three jet cross section can be used for precision phenomenology, e.g. the simultaneous determination of α_s and PDF's from experimental data. Together with the inclusive jet and dijet cross sections the results for α_s and the PDF's get then partially decorrelated.

usually "fulfill"

The leading transverse momentum jet has to fulfil $p_T > 150$ GeV and the third leading transverse momentum jet $p_T > 40$ GeV. The leading jets are restricted to $|y| < 0.8$, $|y| < 1.6$, $|y| < 2.4$ in three different measurements. Two additional measurements are made for third leading jet $p_T > 70$ GeV and $p_T > 100$ GeV, rapidity $|y| < 2.4$. The cone jet algorithm [3] with radius $R = 0.7$ is used and all pairs of the three leading jets are required to be spatially separated by $\Delta R > 1.4 (= 2 \cdot R)$. Dominating systematic uncertainty on the cross section is given by the Jet Energy Scale (JES) with 10 - 15% for $|y| < 0.8$ and 10 - 30% for $|y| < 2.4$. The p_T resolution for jets is about 15% at 40 GeV, decreasing to below 10% at 400 GeV. The corresponding uncertainty on the cross section amounts to 1 - 5%. The uncertainty on the luminosity contributes with 6.1%. In Fig. 1 the data over theory prediction ratios of the differential cross section $d\sigma_{3\text{jet}}/dM_{3\text{jet}}$ are shown in the different rapidity regions and for different third jet transverse momentum thresholds. The MSTW2008NLO PDF uncertainties

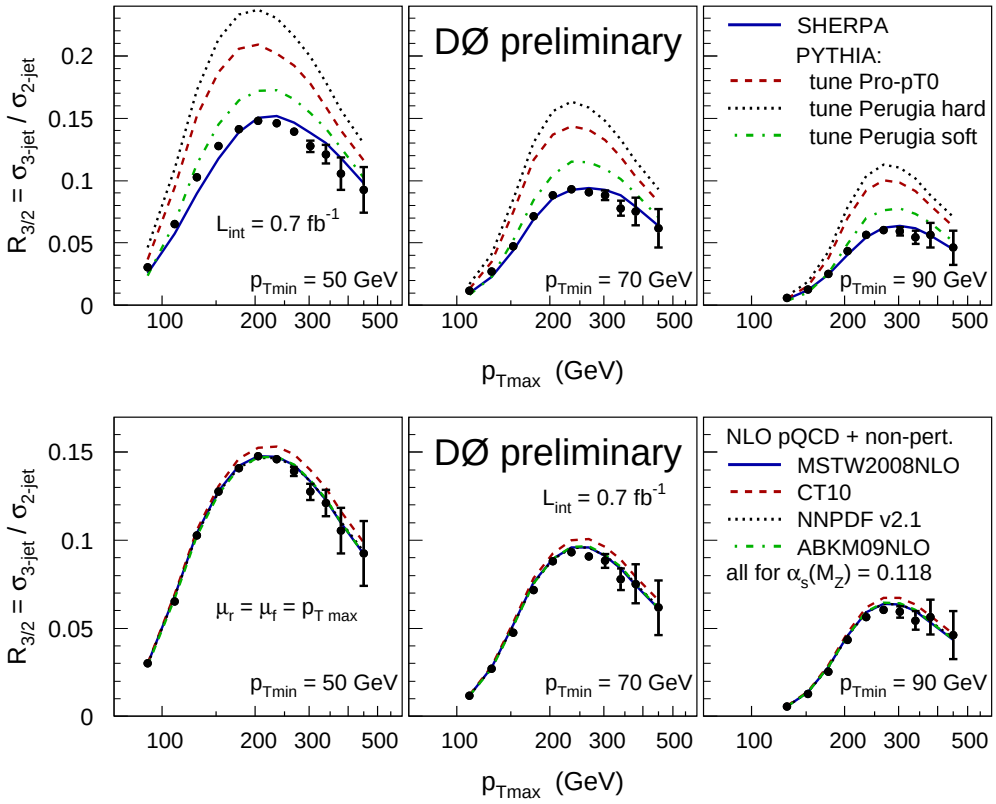

Figure 2. Trijet inclusive over dijet inclusive cross section ratio as a function of the leading transverse momentum jet in comparison to various predictions of SHERPA and PYTHIA (top) and next-to-leading order pQCD calculations (bottom).

corresponding to the 68% C.L. are shown by the light band. Normalised to MSTW2008NLO, the CT10 PDF's[23] with corresponding value of $\alpha_s(M_Z) = 0.118$ predict a different shape with increasing discrepancy at higher invariant masses.

2.4. Ratio of inclusive trijet/dijet production $R_{3/2}$

The ratio $R_{3/2}$ of inclusive trijet over dijet production is measured [28] as a function of the leading jet transverse momentum $p_{\max}$ based on an integrated luminosity of 0.7 fb^{-1}. Jet production is sensitive to the dynamics of the fundamental interaction and the partonic structure of the initial state hadrons. Measurements dedicated to investigate the interaction dynamics are preferentially based on observables which are insensitive to the PDF's. Such observables can be constructed as ratios of cross sections for which the PDF sensitivity cancels. The ratio R_{32} of inclusive trijet over inclusive dijet production is such an observable. In the R_{32} measurement reported here α_s is being probed up to jet transverse momenta of 500 GeV. Jets are defined by the cone algorithm [3] with radius $R = 0.7$ and all pairs of n-leading jets ($n = 2, 3$) are required to be separated by $\Delta R > 2 \cdot R$. The cross section ratio is determined in three bins of jet transverse momentum thresholds $p_T^{\min} > 50$, 70, 90 GeV. The leading transverse momentum jet has to exceed the n-th leading jet by $p_T^{\max} > p_T^{\min} + 30$ GeV to ensure sufficient phase space for the second and third leading jet such that corrections due to the experimental p_T resolution remain small. In Fig. 2 (top) the cross section ratio is compared to the event generators SHERPA 1.1.3 [29] and PYTHIA 6.419 [27] for three different tunes using a p_T-ordered parton shower. The MSTW2008LO PDF's have been deployed for the predictions of both event generators. While SHERPA with leading order matrix elements for 2-, 3- and 4-jet production matched to parton shower describes the data well, PYTHIA with tunes using the p_T-ordered parton shower is not able to describe the data. PYTHIA making use of the tune BW with Q^2-ordered parton shower is able to describe the data but a former DØ measurement of dijet azimuthal decorrelations [30] can not be described by the BW tune. As can be seen in Fig. 2 (bottom) the prediction of pQCD in next-to-leading order is describing the data very well. PYTHIA predicts non-perturbative corrections due to hadronisation and underlying event of 2.5% $\pm$ 0.5%. Therefore the discrepancies of various tunes can not be explained by poor parameter choices for the hadronisation and/or underlying event models. It can only be explained by parameters which affect the perturbative physics as implemented in the parton shower or by a fundamental limitation of the model itself.

3. Vector boson plus jet production

Measurements of vector boson plus jet production provide fundamental tests of pQCD in particular at high momentum scales. Furthermore these kind of processes can constitute the dominant background in measurements of single top quark and $t\bar{t}$ production as well as in searches for the Standard Model (SM) Higgs boson and for physics beyond the SM. In particular Z boson plus b jet production is an important background for associated Standard Model Higgs boson production ($ZH \to Zb\bar{b}$) and also supersymmetric partners of b quarks. Furthermore the b quark density of the proton can be probed.

3.1. Inclusive Z boson cross section ratio $\sigma(p\bar{p} \to Z + b + X)/\sigma(p\bar{p} \to Z + j + X)$

The ratio of the inclusive production of a Z boson accompanied by a b jet over the inclusive production of a Z boson accompanied by a light flavoured jet $\sigma(p\bar{p} \to Z + b + X)/\sigma(p\bar{p} \to Z + j + X)$ is measured [31] as a function of the leading jet transverse momentum based on an integrated luminosity of 4.2 fb^{-1}. The measurement of the cross section ratio benefits from cancellations of many systematic uncertainties.

Selected events are required to pass at least one of the single electron or single muon triggers. A Z boson candidate with an invariant dilepton mass of $70 < m_{\ell\ell} < 110$ GeV has to be reconstructed. Electrons (muons) have to have a transverse momentum of $p_T > 15$ GeV ($p_T >$

10 GeV). Electron candidates are built from isolated energy deposits in the electromagnetic calorimeter with a shower shape consistent to that expected from electrons. Combined tracking and calorimeter isolation requirements are applied to the muon candidates. At least one jet with $p_T > 20$ GeV and further jets with $p_T > 15$ GeV, making use of the midpoint cone algorithm [3] with cone radius $R = 0.5$ are required. Jets with b content have a different energy response and receive an additional average energy correction of about 6%. The b-tagging algorithm is based on a neural network exploiting the longer lifetime of b-flavoured hadrons which result in tracks with sizeable impact parameters and secondary vertices. The necessary tracks associated to jets have to exceed a transverse momentum of 0.5 GeV and 1.0 GeV for the leading track. At least one of the jets has to be b-tagged. The tagging efficiency for b jets and light jets are parameterised as functions of jet p_T and pseudorapidity η. They amount to about 58% and 2% respectively. To further separate b jets from c and light jets a discriminant based on the secondary vertex mass M_{SV} and the jet lifetime impact parameter (JLIP) is introduced. Events with missing transverse energy $\not{E}_T > 60$ GeV are rejected to suppress background from $t\bar{t}$ production. The dominant background to Z + jet production arises from multijet events with jets misreconstructed as leptons, especially in the ee channel. Smaller background contributions arise from $t\bar{t}$ and diboson (ZW, ZZ, WW) production. A binned maximum likelihood fit to the discriminant distribution in data using a linear combination of light, c and b flavoured jet templates from simulation is performed to determine the flavour fractions. Several experimental uncertainties cancel out in the measurement of the cross section ratio $\sigma(Z+b+X)/\sigma(Z+j+X)$, including the uncertainties on the luminosity, trigger, lepton identification and some jet identification efficiencies. The two largest remaining sources of systematic uncertainty are due to the discriminant efficiency and the shape of the discriminant templates. Other important sources of uncertainty are the b-tagging efficiency with 2.4%, the b jet energy scale with 2% and reconstruction efficiency with 3.2%. The measurement of the ratio yields $\frac{\sigma(Z+b\text{jet})}{Z+]\text{jet}} = 0.0193 \pm 0.0022(\text{stat}) \pm 0.0015(\text{syst})$ consistent with the ratios obtained separately in the two lepton channels and the NLO prediction of MCFM [32] of 0.0192 ± 0.0022 obtained for renormalisation and factorisation scales $\mu_R^2 = \mu_F^2 = m_Z^2$ making use of the MSTW2008 [12] PDF's.

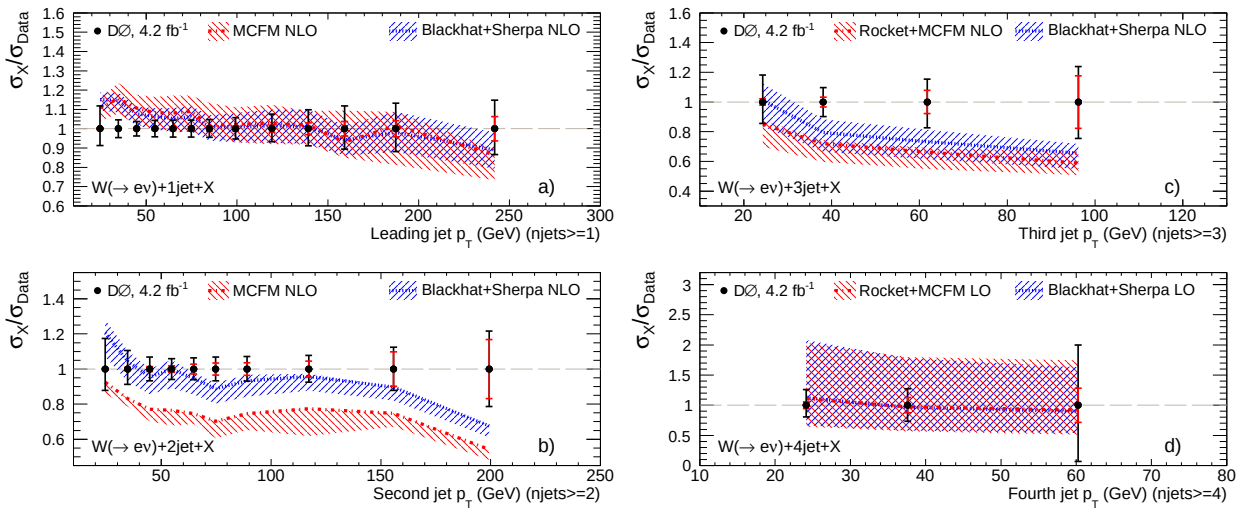

Figure 3. Ratio of pQCD predictions to measured differential cross section for the p_T of the n-th leading jet in $W + n$ jet production (left: $n = 1$ (top), $n = 2$ (bottom). Right: $n = 3$ (top), $n = 4$ (bottom)). The shaded areas indicate the theoretical uncertainties due to variations of the factorisation and renormalisation scales.

I would change to "as a function" instead of "in dependence"

3.2. Inclusive $W(\to e\nu_e)$ plus jets production rates

The inclusive W boson plus jets production rates are measured [36] in dependence of the inclusive number of jets based on an integrated luminosity of 4.2 fb^{-1}. The results are corrected to the hadronic final state in deconvolving the effects of finite detector resolution, detector response, acceptance and efficiencies. Jets are identified with the DØ midpoint cone algorithm [3] with cone radius $R = 0.5$. Jet energy corrections are determined by means of the transverse momentum imbalance in γ + jet events, where the electromagnetic calorimeter response is calibrated using $Z/\gamma^* \to e^+e^-$ events. The missing transverse energy $\not{E}_T$ is corrected for the presence of any muon in the event. Central electrons with $p_T > 15$ GeV, missing transverse energy $\not{E}_T > 20$ GeV, transverse mass of the W boson candidate event $M_T^W > 40$ GeV and jet transverse momenta of $p_T > 20$ GeV are required. Furthermore, the distance between electrons and the nearest jet has to satisfy $\Delta R > 0.5$ in azimuthal angle ϕ and pseudorapidity η space. After this selection there are backgrounds from Z + jets, $t\bar{t}$, diboson, single top quark and multijet production. W/Z+jets and $t\bar{t}$ processes are simulated with ALPGEN v2.11 [38], interfaced to PYTHIA v6.403 [37] for the simulation of initial and final state radiation and for the hadronisation. The PYTHIA event generator is used to simulate diboson production. Single top quark production is simulated via the COMPHEP [33] generator interfaced to PYTHIA. The cross sections for W/Z + jet production used for acceptance and smearing corrections are simulated by ALPGEN, corrected with a constant factor to match the inclusive W/Z + jet cross section calculated at NLO [34][35]. Additional corrections are applied to W/Z + heavy flavour jet production to match the prediction of NLO calculations. Multijet background is determined by means of a data-driven method [39] in which data in a control region orthogonal to the data selection is used to determine shape and overall normalisation of the multijet contribution. After background subtraction the data are unfolded, including an unfolding bias correction of the order 0.5 - 2%. All differential cross section measurements are normalised to the measured inclusive W boson cross section. The total inclusive W boson cross section is measured to be $\sigma_W = 1132 \pm 1(\text{stat})^{+43}_{-84}(\text{syst}) + 69(\text{lumi})$ pb. A recent publication [40] of $W + 4$ jet production at NLO for pp collisions at $\sqrt{s} = 7$ TeV is available. These predictions are not available for the Tevatron. Comparisons with theory are therefore limited to LO for $W + 4$ jet production. For the predictions up to three partons in the final state the partonic final state generators BLACKHAT [41], interfaced to SHERPA [29] and ROCKET [42] interfaced to MCFM [32] are used. BLACKHAT + SHERPA deploys the renormalisation and factorisation scale $\mu = \mu_R = \mu_F = \frac{1}{2}\hat{H}_T$ where $\hat{H}_T$ is the scalar sum of parton and lepton transverse energies. The choice made by the ROCKET + MCFM authors is $\mu = \sqrt{M_W^2 + \frac{1}{4}(\sum p^{\text{jet}})^2}$ in the $n = 2, 3$ and 4 jet bins. In the 1 jet bin the factor 1/4 is omitted. The PDF's used for the theory calculations are MSTW2008 [12]. Hadronisation corrections are obtained with SHERPA and the CTEQ6.6 PDF's. Fig. 3 shows ratio of the pQCD predictions to the differential cross sections for W boson plus jet production in the jet multiplicity bins $n = 1 - 4$ as a function of the n-th jet transverse momentum respectively. The BLACKHAT + SHERPA predictions are in very good agreement with the data everywhere except at small jet p_T. The ROCKET + MCFM predictions are significantly below the data. In particular the difference in the $W + 2$ jet bin indicates that the scale uncertainties are larger than determined. The data offers here guidance on good choices of the renormalisation and factorisation scales.

4. Direct photon production

Direct photons come unaltered from the hard subprocess and provide therefore a direct probe of the hard scattering dynamics. The energy calibration of photons is better than the energy calibration of jets. Direct photons are also important background to many physics processes. At the same time the cross section of multijet production dominates. Therefore the understanding

of the QCD production mechanism is indispensable in search for new physics.

Photon candidates are given by electromagnetic showers in the calorimeter. By means of shower profile and geometric isolation criteria they are distinguished from background, such as neutral mesons and jets with high electromagnetic fraction. No associated track has to be found and jets have to be separated by a geometrical distance of $\Delta R > 0.7$ in (η, ϕ)-space. Multiple preshower hits help to distinguish prompt photons from $\pi^0 \to 2\gamma$ decays.

At low photon transverse momentum ($p_T^\gamma < 120$ GeV) photon + jet production through Compton scattering $qg \to q\gamma$ dominates. The requirement of isolated photons reduces the contribution of photon fragmentation of quarks. Photon + jet production can be exploited to probe PDF's at low x (down to $x \simeq 0.007$ at the Tevatron), where quarks are constrained by HERA data and therefore one is sensitive to the gluon density. Finally pQCD can be probed at NLO, including soft gluon resummation and models of gluon radiation.

4.1. Inclusive photon plus jet production

The inclusive photon plus jet production is measured [43] as a function of the photon transverse momentum based on an integrated luminosity of 1.0 fb^{-1}. An isolated central photon with $p_T > 30$ GeV is required to pass a neural network background discrimination based on tracker and calorimeter information. Jets above a transverse momentum of $p_T > 15$ GeV in the two

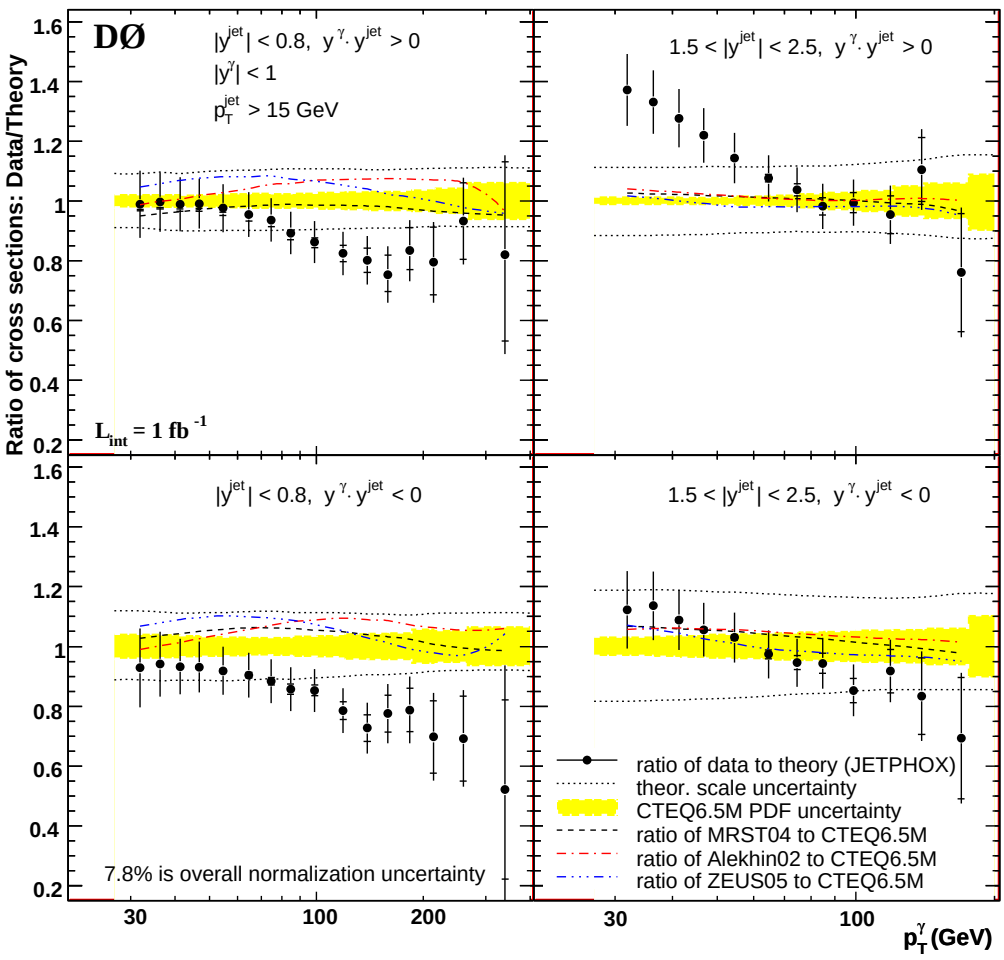

Figure 4. Ratio of measured triple differential cross section for same/opposite photon and jet rapidities and central or forward leading jets as a function of the photon transverse momentum.

rapidity intervals $|y| < 0.8$ (central) and $1.5 < |y| < 2.5$ (forward) are selected. Four regions are distinguished, depending on if the photon and jet have the same or opposite rapidity sign ($y^{\gamma} \cdot y^{\text{jet}} < 0$ or > 0) and depending on the central or forward location of the leading jet. The triple differential cross section as a function of the photon transverse momentum and rapidity and the jet rapidity $d^3\sigma/dp_T^{\gamma}dy^{\gamma}dy^{\text{jet}}$ is measured. The NLO prediction is given by JETPHOX [44][45] making use of CTEQ6.5 [8] PDF's and BFG photon fragmentation functions [46]. In Fig. 4 the triple differential cross section is shown for the four different phase space regions, depending on the same/opposite photon jet hemisphere and the central/forward leading jet location as a function of the photon transverse momentum. The theory is not able to describe the data in the whole measured range. The structure is similar to previous observations of UA2 [47], CDF [48] and DØ [49][50]. The cross sections as a function of the photon p_T can also be arranged as ratios over two different regions (out of the four possible regions) giving rise to six different ratios which benefit from reduced systematics. The shapes of the measured cross section ratios in data are qualitatively reproduced by the theory in general, but quantitative disagreement is observed for some kinematic regions. This disagreement holds in particular for central jets over same sign rapidity forward jets.

4.2. Inclusive photon plus heavy flavour jet production

The inclusive photon plus heavy flavour jet production is measured [51] as a function of the photon transverse momentum based on an integrated luminosity of 1.0 fb^{-1}. The QCD Compton photo production process dominates for photon transverse momenta of $p_T \sim 90$ (120) GeV for b (c) quark flavour. Since the outgoing quark flavour is for this production mechanism equal to the incoming quark flavour, constraints can be set on the heavy flavour content of the PDF's. At larger photon p_T the quark anti-quark annihilation process with a photon and a gluon dominates, where the gluon splitting into a charge conjugated heavy flavour quark pair enters into the considered data sample. An isolated central photon with transverse momentum of $p_T > 30$ GeV is required together with central jets (cone radius $R = 0.5$) above a transverse momentum of 15 GeV. A neural network is applied to the jets to enhance the heavy flavour content of the selected data sample. Templates for different flavour contents are built by means of a function of jet track probabilities. The distributions of these functions are fitted to the shape of the data to extract the flavour composition. The measurement is done separately in the two kinematic regions given by same and opposite photon and jet rapidities. The cross sections for the b and c quark flavours in the two kinematic regions are measured as a function of the photon transverse momentum. Comparison to theory [52] reveals disagreement for $\gamma + c$ jet production for photon transverse momenta above 70 GeV.

4.3. Direct photon pair production

The direct photon pair production cross section is measured [53] as function of the invariant diphoton mass $M_{\gamma\gamma}$, the azimuthal angle between the two photons $\Delta\phi_{\gamma\gamma}$ and the cosine of the diphoton scattering angle in the diphoton rest frame based on an integrated luminosity of 4.2 fb^{-1}. Direct photon pair production with large invariant mass $m_{\gamma\gamma}$ constitutes a large and irreducible background to searches for the Higgs boson decaying into a pair of photons at hadron colliders. It is also a significant background in searches for new phenomena, such as new heavy resonances [54], extra spatial dimensions [55], or cascade decays of heavy new particles [56]. Double photon production is also interesting to check the validity of pQCD and soft gluon resummation implemented in theoretical calculations. Background contributions from single and double photon fragmentation are suppressed by photon isolation and invariant $m_{\gamma\gamma}$ requirements, which entails smaller theoretical uncertainties. Events with two central isolated photons of transverse momentum $p_T^{\gamma_1} > 21$ GeV and $p_T^{\gamma_2} > 20$ GeV are selected with unbalanced thresholds to ensure non-vanishing phase space at NLO. The invariant mass is required to

exceed the transverse momentum of the diphoton system $m_{\gamma\gamma} > p_T^{\gamma\gamma}$. The two photons have to be separated by the distance $\Delta R > 0.4$ in (η, ϕ)-space. The cross sections are measured differentially as a function of $m_{\gamma\gamma}$, the diphoton transverse momentum $p_T^{\gamma\gamma}$, the azimuthal angle between the photons $\Delta\phi_{\gamma\gamma}$ (see Fig. 5 for a comparison to theory and various models) and the cosine of the scattering angle $\cos\theta^* = \tanh[(\eta_1 - \eta_2)/2]$, where holds $p_T^{\gamma_1} > p_T^{\gamma_2}$. The shapes of the $p_T^{\gamma\gamma}$ and $\Delta\phi_{\gamma\gamma}$ distributions are mostly affected by initial state gluon radiation and fragmentation effects. Furthermore, the $m_{\gamma\gamma}$ spectrum is in particular sensitive to potential contributions from new phenomena. The $\cos\theta^*$ distribution probes PDF effects and the angular momentum of the final state. The measured cross sections are compared to theoretical predictions from RESBOS [57][58], DIPHOX [59] and PYTHIA [60]. Both, RESBOS and DIPHOX provide pQCD NLO predictions, however the $gg \to \gamma\gamma$ contribution is implemented only at leading order (LO) in DIPHOX. The explicit parton-to-photon fragmentation functions are included in DIPHOX at NLO, while in RESBOS a function approximating rates from NLO fragmentation diagrams is introduced. Furthermore only in RESBOS the effect of soft and collinear initial state gluon emission is resummed to all orders. The normalisation uncertainty on the measured cross section amounts to 7.4% due to uncertainties on the luminosity of 6.1% and on the selection criteria of 4.3%. PDF uncertainties are determined by means of DIPHOX, making use of the CTEQ6.6M [14] PDF's. The renormalisation, factorisation and fragmentation scales are set to $\mu_R = \mu_F = \mu_f = m_{\gamma\gamma}$. Studies performed using DIPHOX indicate that the contribution to the overall cross section from one- and two-photon fragmentation processes does not exceed 16% and significantly drops at large $m_{\gamma\gamma}$, $p_T^{\gamma\gamma}$ and small $\Delta\phi_{\gamma\gamma}$ to 1 - 3%. None of the theoretical predictions considered is able to describe the data well in all kinematic regions of the four variables. RESBOS shows the best agreement with data, although systematic discrepancies are observed at low $m_{\gamma\gamma}$, high $p_T^{\gamma\gamma}$ and low $\Delta\phi_{\gamma\gamma}$. The large discrepancy between RESBOS and DIPHOX in some regions of the phase space is due to the absence of all-order soft gluon resummation and the LO approximation of the $gg \to \gamma\gamma$ contribution in DIPHOX. Further insight can be obtained in considering double differential cross sections. Therefore the differential cross sections as functions of $p_T^{\gamma\gamma}$, $\Delta\phi_{\gamma\gamma}$ and $|\cos\theta^*|$ are measured in three invariant $m_{\gamma\gamma}$ mass bins 30 - 50 GeV, 50 - 80 GeV and 80 - 350 GeV. The largest discrepancies between data and RESBOS are found for each kinematic variable in the lowest $m_{\gamma\gamma} < 50$ GeV region. This is the region, where the contribution of $gg \to \gamma\gamma$ is expected to be largest. Finally, the addition of NNLO corrections to RESBOS remains to be compared.

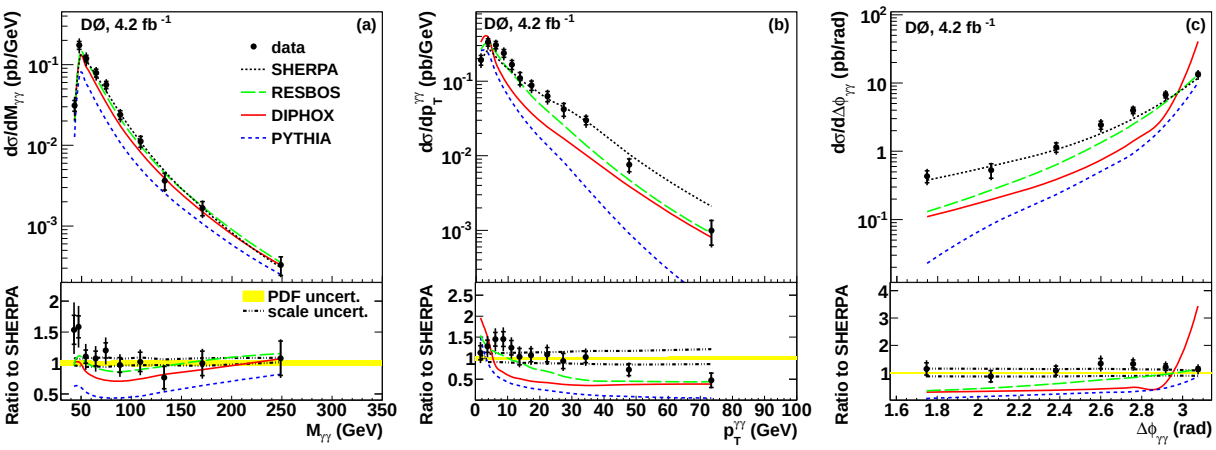

Figure 5. Differential diphoton production cross section as a function of the invariant diphoton mass $m_{\gamma\gamma}$ (a), the transverse diphoton momentum $p_T^{\gamma\gamma}$ (b) and the azimuthal angle between the photons $\Delta\phi_{\gamma\gamma}$ (c).

5. Minimum bias and double parton scattering

The non-perturbative nature of low energy QCD processes makes it necessary to develop heuristic descriptions. Models that describe these soft processes are implemented in Monte Carlo event generators. They contain many parameters that need to be tuned using experimental input. Most prominent input observables are charged particle multiplicities and track mean transverse momenta.

Double Parton Scattering (DPS) may constitute a background for many rare processes of interest, especially those with multi-jet final states. The measurement of DPS provides complementary information about the proton structure in terms of the spatial distributions of partons. Furthermore it allows one to probe for parton-parton correlations and therefore to check for a possible impact on the PDF's. Multiple Parton Interaction (MPI) models can be constrained and improved taking DPS measurements into account.

5.1. ϕ and η correlations in minimum bias events

The azimuthal angle and pseudorapidity correlations in minimum bias events are measured [61] based on a data set taken in the years 2002 to 2006. Complementary to existing observables the azimuthal angle difference $\Delta\phi$ between the highest transverse momentum track and any other track in a given event is considered here. This observable has the advantage of being as independent as possible of the track fake rate and the tracking efficiency. The general shape of of the $\Delta\phi$ distribution consists of peaks at 0 and π on top of a pedestal of a certain height.

Events with more than one reconstructed proton anti-proton interaction per bunch crossing are selected and the single collision that fired the trigger is being identified. The remaining collisions of the same bunch crossing are regarded as minimum bias events. The triggers used are dimuon triggers. The primary vertices of these collisions are required to have at least five tracks with transverse momentum above 0.5 GeV inside the geometrical tracker acceptance ($|\eta| < 2$). Long-lived particles, such as pions and K_s are discriminated by means of a vertex χ^2 requirement based on three dimensional track impact parameter significances. Uncorrelated fake tracks and wrongly associated real tracks are distributed uniformly in $\Delta\phi$. This flat background is eliminated in fitting the distribution by a polynomial and subtracting the height at minimum from the whole distribution. The absolute level of the shape of the $\Delta\phi$ distribution is affected by the tracking efficiency but the dependence is minimised by normalising the distribution to unit area and only considering the shape. As it turned out it has not been necessary to unfold the experimental result. A further observable has been defined by assigning the tracks into two pseudorapidity regions based on the sign of the leading tracks η. The remaining tracks belong then to the same or opposite region depending on the sign of their η respectively. The number of same sign tracks subtracted by the number of opposite sign tracks in a given $\Delta\phi$ bin, normalised to the sum of all such expressions over all $\Delta\phi$ bins is then the final observable which is being considered as a function of $\Delta\phi$. The observables are compared to three PYTHIA tune and model implementations, which are Rick Field's Tune A [62], the Perugia 0 tune (P0) [63] and the Generalised Area Law model of colour reconnections (GAL) [64]. Tune A is historically significant and makes use of Q^2-ordered parton showers while the more recent tune P0 makes use of p_T ordered showers. Both use the colour annealing model for colour reconnections. GAL is based on the tune S0 [65] but uses the Generalised Area Law colour reconnection model. The different tunes show large differences for the considered observables which provide therefore important additional information to be taken into account in tunes.

5.2. Double parton scattering in γ + 3 jet events

The double parton scattering fraction is measured [66] in dependence of the second leading jet transverse momentum based on an integrated luminosity of 1.0 fb^{-1}. The cross section for DPS is given by $\sigma_{DP} = m \cdot \frac{\sigma_A \sigma_B}{2\sigma_{\text{eff}}}$, where σ_A and σ_B are the cross sections of the processes A and

Model	$\rho(r)$	σ_{eff}	R_{rms}	R_{rms} (fm)
Solid sphere	const., $r < r_p$	$4\pi r_p^2/2.2$	$\sqrt{3/5}r_p$	0.41 ± 0.05
Gaussian	$e^{-r^2/2a^2}$	$8\pi a^2$	$\sqrt{a}$	0.44 ± 0.05
Exponential	$e^{-r/b}$	$28\pi b^2$	$\sqrt{12}b$	0.47 ± 0.06

Table 1. Parameters of different spatial parton density models calculated from σ_{eff}.

B, m is a constant permutation factor which corresponds to one in case of indistinguishable processes A and B. It assumes the value $m = 2$ in the case of distinguishable processes A and B as discussed here. σ_{eff} is a process independent scaling parameter which gives a measure for the size of the effective interaction region. The expression $\sigma_B/2\sigma_{\text{eff}}$ can be interpreted as the probability of a second interaction B given that a first one A has taken place.

DPS is measured in $\gamma + 3$ jet events which benefits from the better energy measurement of the photon and a larger fraction of Double Parton (DP) events compared to 4-jet events [67]. Events with an isolated high transverse momentum photon of $60 < p_T < 80$ GeV are selected to increase the photon purity. Furthermore this requirement ensures a clean separation of the jet produced in the same parton scattering and jets produced by a different scattering. The jet transverse momenta are corrected to the hadronic final state. The first jet in transverse momentum is required to fulfil $p_T > 25$ GeV and the second and third jet $p_T > 15$ GeV. Jets are reconstructed with the iterative midpoint cone algorithm [3] with cone size $R = 0.7$. The main background is Single Parton (SP) scattering. Also Double Interaction (DI) events with two scatterings of two different $p\bar{p}$ collisions in the same bunch crossing (referred to as pile-up) have to be considered. They can be distinguished by the separate collision vertex. The contribution from single and double diffraction events represents $< 1\%$ of the total dijet cross section. The p_T spectrum for jets from dijet production falls faster than that for jets resulting from initial or final state radiation in the $\gamma+$ jets events. Therefore DP fractions depend on the jet p_T and the DP fractions as well as σ_{eff} can be determined in data by a set of equations, relating the different contributions in the three second jet transverse momentum bins 15 - 20, 20 - 25 and 25 - 30 GeV. In each momentum bin the discriminating variables $S_{p_T} = \frac{1}{\sqrt{2}}\sqrt{\left(\frac{|\vec{P_T}(\gamma,i)|}{\delta P_T(\gamma,i)}\right)^2 + \left(\frac{|\vec{P_T}(j,k)|}{\delta P_T(j,k)}\right)^2}$, $S_{p'_T} = \frac{1}{\sqrt{2}}\sqrt{\left(\frac{|\vec{P_T}(\gamma,i)|}{|\vec{P}_T^{\gamma}|+|\vec{P}_T^{i}|}\right)^2 + \left(\frac{|\vec{P_T}(j,k)|}{|\vec{P}_T^{j}|+|\vec{P}_T^{k}|}\right)^2}$ and $S_\phi = \frac{1}{\sqrt{2}}\sqrt{\left(\frac{\Delta\phi(\gamma,i)}{\delta\phi(\gamma,i)}\right)^2 + \left(\frac{\Delta\phi(j,k)}{\delta\phi(j,k)}\right)^2}$ are evaluated, where ϕ is the azimuthal angle and δ indicates the uncertainty of a given variable, defined between pairs of photon (γ) and jet (i, j, k) objects. These variables are computed for the reconstructed particle pairing which minimises S. For this pairing and each variable the final observable $\Delta S = \Delta\phi(\vec{P}_T(\gamma, i), \vec{P}_T(j, k))$ is being determined.

The measurement reveals that the DP fraction drops from 0.47 in the second jet $15 < p_T < 20$ GeV transverse momentum bin to 0.23 in the second jet $25 < p_T < 30$ GeV transverse momentum bin. Averaging over the three second jet transverse momentum bins yields $< \sigma_{eff} >= 16.4 \pm 0.3(\text{stat}) \pm 2.3(\text{syst})$ mb. Good agreement with previous CDF measurements in 4-jet [68] and γ+3 jet [69][70] events are observed. From the parameter σ_{eff} the proton radius in different parton spatial density models (see Table 1) can be calculated.

5.3. Azimuthal decorrelations and double parton scattering in γ + 2 jet and γ + 3 jet events

The azimuthal decorrelations and double parton scattering in $\gamma + 2$ jet and $\gamma + 3$ jet events are measured [71] based on an integrated luminosity of 1.0 fb^{-1}. This analysis provides an extension of the DPS analysis discussed above in allowing also for $\gamma + 2$ jet events, where a third jet is not reconstructed or did not pass the selection criteria. The gained statistics allows one to subdivide the cross section measurement in bins of the second jet transverse momentum and increases in

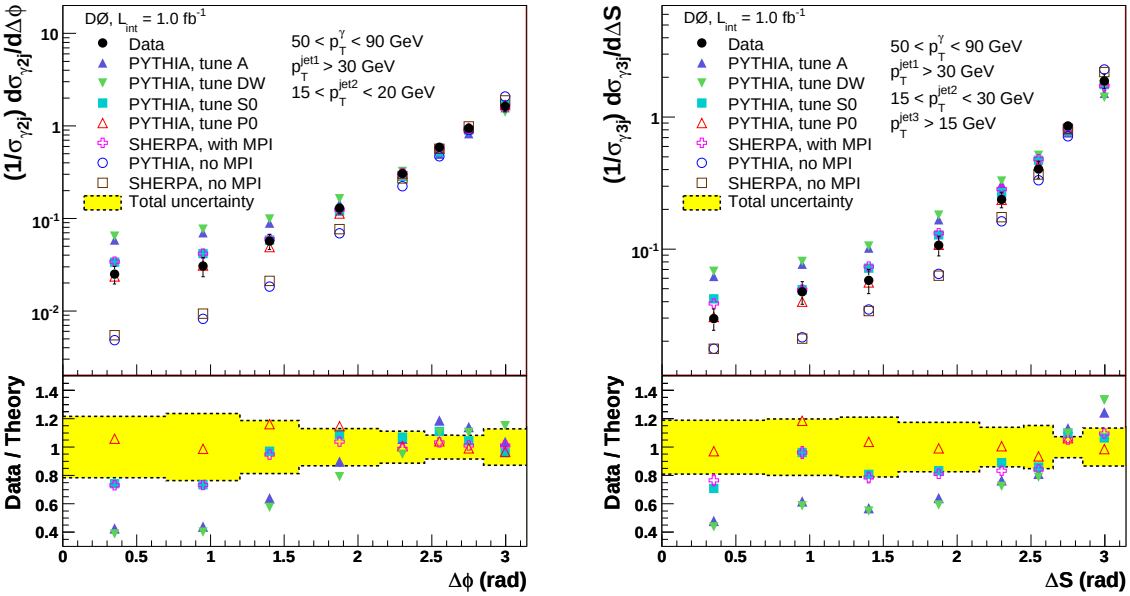

Figure 6. Differential cross section in $\gamma + 2$ jet events as a function of $\Delta\phi$ (left) and differential cross section in $\gamma + 3$ jet events as a function of ΔS (right) in the second leading jet bin respectively. The data is compared to various models.

this way the sensitivity to MPI models.

Events with an isolated high transverse momentum photon of $50 < p_T < 90$ GeV are selected. The jet transverse momenta are corrected to the hadronic final state. The first jet in transverse momentum is required to fulfil $p_T > 30$ GeV and one or two more jets with $p_T > 15$ GeV have to be found. Jets are reconstructed with the iterative midpoint cone algorithm [3] with cone size $R = 0.7$. The event selection for photons and jets is identical to the requirements of the previous analysis discussed above. In addition a separation requirement between any pair of selected objects among the photon and the jets of $\Delta R > 0.9$ is used. The sample of DP candidates is selected from events with a single reconstructed $p\bar{p}$ collision vertex. For $\gamma + 2$ jet events the differential cross section as a function of the azimuthal angle difference between the photon + leading p_T jet system and the second leading p_T jet $\Delta\phi(\gamma + \mathrm{jet}_1, \mathrm{jet}_2)$ is considered in three bins of second leading p_T jet 15 -20 (see Fig. 6, left), 20 - 25 and 25 - 30 GeV. For $\gamma + 3$ jet events the differential cross section as a function of the azimuthal angle difference between the photon + leading p_T jet system and the second + third leading p_T jet $\Delta S = \Delta\phi(\vec{P}_T(\gamma, \mathrm{jet}_1), \vec{P}_T(\mathrm{jet}_2, \mathrm{jet}_3))$, for statistical reasons only in a single 15-30 GeV second transverse momentum jet bin (see Fig. 6, right). The differential cross sections are normalised for an improved sensitivity to MPI models. Various models and tunes of PYTHIA [60] and SHERPA [29] compared to the data. There are large differences between the models and the data confirm the presence of DP events. The data are close to Perugia (P0) [63], S0 [65] and SHERPA [29] with MPI tunes, while predictions from previous PYTHIA MPI models with tunes A and DW, making use of Q^2-ordered parton showers, are disfavoured.

6. Conclusions

A multitude of DØ measurements in the regime of perturbative and non-perturbative QCD has been elaborated and confronted to theory predictions. While pQCD predictions are in general in agreement with the various measurements, limitations of the non-perturbative parts (e.g. PDF's, photon fragmentation, hadronisation, underlying event) can not be hidden and the experimental results can be exploited to optimise the phenomenological models and their uncertainties.

[1] DØCollaboration, Nucl. Instrum Methods Phys. Res., Sect. A **565**, 463 (2006).
[2] DØ Collaboration, Phys. Rev. Lett. **101**, 062001 (2008).
[3] G. C. Blazey *et al.*, in Proceedings of the Workshop: "QCD and Weak Boson Physics in Run II", edited by U. Baur, R. K. Ellis and D. Zeppenfeld, Batavia, Illinois (2000) p. 47.
[4] C. Buttar *et al.*, arXiv:hep-ph/0803.0678 (2008).
[5] E. J. Eichten, K. D. Lane, M. E. Peskin, Phys. Rev. Lett. **50**, 811 (1983).
[6] T. Kluge, K. Rabberts, M. Wobisch, arXiv:hep-ph/0609285 (2006).
[7] Z. Nagy, Phys. Rev. D **68**, 094002 (2003).
[8] W. K. Tung *et al.*, JHEP **0702**, 053 (2007).
[9] J. Pumplin *et al.* JHEP **0207**, 12 (2002).
[10] D. Stump *et al.*, JHEP **0310**, 046 (2003).
[11] DØ Collaboration, Phys. Lett. **B 693**, 531 (2010).
[12] A. D. Martin, W. J. Stirling, R. S. Thorne, G. Watt, Eur. Phys. J. C 63, 189 (2009).
[13] Z. Nagy, Phys. Rev. Lett. 88, 122003 (2002).
[14] P. M. Nadolsky *et al.*, Phys. Rev. D 78, 013004 (2008).
[15] DØ Collaboration, arXiv:1104.1986, submitted to Phys. Lett. **B** (2011).
[16] CDF Collaboration, Phys. Rev. D **75**, 092006 (2007) [Erratum-ibid. D **75**, 119901 (2007)].
[17] CDF Collaboration, Phys. Rev. D **78**, 052006 (20080) [Erratum-ibid. D **79**, 119902 (2009)].
[18] CDF Collaboration, Phys. Rev. D **79**, 112002 (2009).
[19] DØ Collaboration, Phys. Rev. Lett. **103**, 191803 (2009).
[20] DØ Collaboration, Phys. Lett. B **693**, 531 (2010).
[21] DØ Collaboration, Phys. Rev. D **80**, 111107 (2009).
[22] A. D. Martin *et al.*, Eur. Phys. J. C **63**, 189 (2009).
[23] H. L. Lai *et al.*, Phys. Rev. D **82**, 074024 (2010).
[24] R. D. Ball *et al.*, arXiv:1101.1300 [hep-ph] (2011).
[25] W. B. Kilgore and W. T. Giele, arXiv:hep-ph/9903361; arXiv:hep-ph/0009176; arXiv:hep-ph/0009193.
[26] W. B. Kilgore and W. T. Giele, Phys. Rev. D **55**, 7183 (1997).
[27] T. Sjöstrand and P. Z. Skands, Eur. Phys. J. C **39**, 129 (2005).
[28] DØ Collaboration, DØ conference note 6032-CONF (2011).
[29] T. Gleisberg *et al.*, JHEP **0902**, 007 (2009).
[30] DØ Collaboration, Phys. Rev. Lett. **94**, 221801 (2005).
[31] DØ Collaboration, FERMILAB-PUB-10-435-E, accepted by Phys. Rev. D Rap. Comm. (2011).
[32] J. M. Campell, R. K. Ellis, F. Maltoni and S. Willenbrock, Phys. Rev. D **69**, 074021 (2004).
[33] E. Boos *et al.* (CompHEP Collaboration), Nucl. Instrum. Meth. Phys. Res. A **534**, 250 (2004).
[34] J. Campbell and R. K. Ellis, Phys. Rev. D **65**, 113007 (2002).
[35] D. Rainwater, Phys. Rev. D **68**, 094021 (2003).
[36] DØ Collaboration, Fermilab-PUB-11/246-E, arXiv:1106.1457 [hep-ex], submitted to Phys. Lett. **B** (2011).
[37] T. Sjöstrand *et al.*, Comput. Phys. Commun. **135**, 238 (2001).
[38] M. L. Mangano *et al.*, J. High Energy Phys. **07**, 001 (2003).
[39] DØ Collaboration, Phys. Rev. D **76**, 092007 (2007).
[40] C. F. Berger *et al.*, Phys. Rev. Lett. **106**, 092001 (2011).
[41] C. F. Berger *et al.*, ar4Xiv:0905.2735 [hep-ph] (2009).
[42] R. K. Ellis *et al.*, J. High Energy Phys. **0901**, 012 (2009).
[43] DØ Collaboration, Phys. Lett. **B 666**, 435 (2008).
[44] P. Aurenche *et al.*, Nucl. Phys. **B297**, 661 (1998).
[45] S. Catani *et al.*, JHEP **05**, 028 (2002).
[46] L. Bourhis, M. Fontannaz and J. P. Guillet, Eur. Phys. J. C **2**, 529 (1998).
[47] UA2 Collaboration, Phys. Lett. B **263**, 544 (1991).
[48] CDF Collaboration, Phys. Rev. D **65**, 112003 (2003).
[49] DØ Collaboration, Phys. Lett. B **639**, 151 (2006).
[50] DØ Collaboration, Phys. Lett. B **658**, 285 (2007).
[51] DØ Collaboration, Phys. Rev. Lett. **102**, 192002 (2009).
[52] T. Stavreva and J. F. Owens, arXiv:0901.3791v1 (2009).
[53] DØ Collaboration, Phys. Lett. **B 690**, 108 (2010).
[54] S. Mrenna, J. Wells, Phys. Rev. D **63**, 015006 (2001) and references theirin.
[55] M. C. Kumar, P. Mathews, V. Ravindran, A. Tripathi, Phys. Lett. B **672**,45 (2009).
[56] G. F. Guidice, R. Rattazzi, Phys. Rep. 322, 419 (1999).
[57] C. Balazs, E. L. Berger, S. Mrenna, C.-P. Yuan, Phys. Rev. D **57**, 6934 (1998).
[58] C. Balazs, E. L. Berger, P. Nadolsky, C.-P. Yuan, Phys. Rev. D **76**, 013009 (2007).

[59] T. Binoth, J.-Ph. Guillet, E. Pilon, M. Werlen, Eur. Phys. J. C **16**, 311 (2000).
[60] T. Sjöstrand, S. Mrenna, P. Z. Skands, JHEP **0605**, 026 (2006). We use PYTHIA version 6.420 with Tune A.
[61] DØ Collaboration, DØ conference note 6054-CONF (2010).
[62] R. D. Field (CDF Collaboration), in the Proceedings of APS/DPF/DPB Summer Study on the Future of Particle Physics (Snowmass 2001), Snowmass, Colorado, 30 Jun. - 21 Jul. (2001), pp. P501.
[63] P. Z. Skands, arXiv:hep-ph/0905.3418 (2009).
[64] J. Rathsman, Phys. Lett. B **452**, 364 (1999).
[65] T. Sjöstrand and P. Z. Skands, Eur. Phys. J. C **39**, 129 (2005).
[66] DØ Collaboration, Phys. Rev. **D 81**, 052012 (2010).
[67] M. Drees and T. Han, Phys. Rev. Lett. **77**, 4142 (1996).
[68] CDF Collaboration, Phys. Rev. D **47**, 4857 (1993).
[69] CDF Collaboration, Phys. Rev. Lett. **79**, 584 (1997).
[70] CDF Collaboration, Phys. Rev. D **56**, 3811 (1997).
[71] DØ Collaboration, arXiv:1101.1509v1, submitted to Phys. Rev. **D** (2011).